The internal and translational energy dependence of molecular condensation coefficients: SF_6 and CCl_4

S. J. Sibener[a] and Y. T. Lee
Department of Chemistry, University of California, and Chemical Sciences Division, Lawrence Berkeley Laboratory, Berkeley, California 94720

(Received 27 September 1993; accepted 30 March 1994)

In this paper we describe a series of beam–surface scattering experiments which examine the internal and translational energy dependence of the molecular condensation probabilities for CCl_4 or SF_6 colliding with their respective condensed phases. It has been conclusively shown that thermal excitation of a polyatomic molecule's rotational and vibrational degrees of freedom can inhibit its probability of sticking upon impact with a cryogenically cooled surface. This effect is most pronounced in the limit of low incident kinetic energy, and essentially vanishes at higher velocities. As part of these experiments, we have also obtained the angular and velocity distributions for reflected SF_6 and Kr which have been used to examine the energy and momentum exchange of these gases with their respective condensed phases. Our findings suggest that heterogeneous laser isotope separation schemes based on precollision molecular excitation may warrant further investigation.

INTRODUCTION

Molecular beam–surface scattering experiments are ideally suited for studying many aspects of gas–surface interactions. Scattered particle angular distributions, velocity distributions, and internal energy distributions can now be obtained from such experiments in which the incident beam can be well defined with respect to its velocity, incident angle, and possibly internal quantum state. The target surface can also be well characterized with respect to its temperature, composition, and crystallographic plane. Perhaps most uniquely, these experiments can yield valuable information on the *initial* interaction between the incident particle and the target surface since the gas–surface interaction potential is sampled by "single collision" scattering events.

In this paper we report surface scattering experiments which have examined the mechanistic details of gaseous condensation. In particular, we have set out to understand whether, and if so to what extent, excitation of a polyatomic molecule's internal degrees of freedom (vibration, rotation) can influence its sticking probability upon collision with a cold surface. This question is of current interest for a variety of reasons. In addition to its obvious fundamental importance in understanding gas–surface collisional energy transfer, an improved understanding of polyatomic gaseous condensation may lead to new schemes for heterogeneous laser isotope separation. Furthermore, it is also desirable to understand how both internal and translational energy influence sticking probabilities as the resulting physisorbed molecules are, in many instances, the precursors to chemically important chemisorbed species. Our goal therefore is to investigate the *microscopic* details of physical adsorption and gas–surface energy exchange mechanisms, which should enable us to improve our understanding of the *macroscopic*, and physically important, process of gaseous condensation.

Both theoretical[1–4] and experimental[4–6] investigations of the internal energy dependence of molecular condensation have previously appeared in the literature. Gochelashvili *et al.*[1] have suggested that the sticking coefficient, S, for polyatomic molecules should be expressed as $S=1-\exp(-E_c/E_{\text{tot}})$ where E_c is the critical adsorption energy and E_{tot} represents the total energy of the incident molecule, $E_{\text{tot}}=E_{\text{trans}}+E_{\text{vib}}+E_{\text{rot}}$. From this expression they infer that the reflection probability difference between selectively excited molecules and unexcited ones may serve as the basis for heterogeneous laser isotope separation. This model is obviously an oversimplification of the complex energy transfer pathways for this process. Basov *et al.*[4] have proposed a model which suggests that local heating of the phonons in the immediate region of an adsorption event (due to deposition of E_{tot}) may lead to reevaporation of the adsorbed entity. This is a highly improbable description of the condensation process. Karlov and Shaitan[2] have proposed that the enhanced reflection probability of excited molecules must critically depend on the efficiency of $V\rightarrow T$ energy exchange during the initial collision event. Finally, Doll[3] has proposed a phenomenological model to describe internal energy effects in condensation phenomena which suggests, based upon adiabaticity arguments, that rotational and low-frequency vibrational excitations will have a significant influence on molecular sticking probabilities. All of the above descriptions, in spite of their simplified nature, do predict that internal excitation should inhibit condensation. Experimentally, much controversy still exists over the existence of internal energy effects during physisorption. Bulk kinetic experiments with CO_2 and CO excited in electrical discharges[4] and with laser excited BCl_3 (Ref. 5) suggest that such effects are significant. However, the internal energy effect reported for laser excited BCl_3 has not been observed in an attempted reproduction of that experiment.[6]

In contrast to the situation for physisorption systems, there has been much activity aimed at quantifying the influence that internal excitation can have on dissociative chemisorption probabilities. Early classical trajectory calculations of Gelb and Cardillo[7] predicted that the probability of H_2

[a]Current address: The James Franck Institute and Department of Chemistry, The University of Chicago, 5640 S. Ellis Avenue, Chicago, IL 60637.

 0021-9606/94/101(2)/1693/11/$6.00

dissociation upon collision with Cu(100) should exhibit a 40-fold increase for $v=1 H_2$ relative to molecules in their ground vibrational state. These calculations, carried out in support of prior dissociative adsorption sticking measurements,[8,9] raised many questions about the nature of the potential energy surfaces for such systems. Subsequent theoretical[10–13] and experimental[14–18] studies have helped clarify the various nuances in the potential energy surfaces and collision dynamics which account for such internal energy effects. Another prototypical molecule in the area of activated chemisorption has been CH_4. Early field emission studies by Stewart and Ehrlich[19] seemed to indicate that thermal vibrational excitation of CH_4 could promote dissociative chemisorption on rhodium (other interpretations of their experimental findings are also possible). Yates *et al.*[20] have shown that laser excitation of the CH_4 ν_3 and (indirectly) $2\nu_4$ and ν_4 modes does not significantly promote its chemisorption on Rh(111). Ehrlich and co-workers[21] have also shown that excitation of methane's ν_3 mode to either its first or second excited level does not actively enhance its probability of dissociative chemisorption on evaporated films of rhodium. Studies involving thermal excited molecular beams of CH_4 indicate the presence of small but measurable vibrational effects in dissociative adsorption.[22,23] The still evolving issue here is to delineate the relative efficacy that excitation of different normal modes have towards dissociative chemisorption, and to use these findings to improve our understanding of chemisorptive potential energy surfaces. Related to this issue are the mechanisms and probabilities by which collision induced energy exchange processes couple internal degrees of freedom (R,V,E) with each other and with the translational coordinate, such as in direct[24] and trapping-desorption[25] mediated scattering.

The experiments presented in this paper have directly confirmed the existence of an internal energy dependence of molecular sticking probabilities for collisions of rotationally and vibrationally excited molecules with a cold surface. We have examined this internal energy dependence as a function of incident translational energy for velocity selected, and thermally excited, molecular beams of CCl_4 and SF_6. A preliminary report of the CCl_4 results has appeared previously.[26] Thermal excitation rather than laser (state-selective) excitation was employed in these studies as the main interest was to establish the presence, and to gauge the extent, of internal energy effects in gaseous condensation. For relatively large polyatomic molecules, such as SF_6, thermal excitation allows us to "excite" virtually all of the incident molecules. Resonant ir laser excitation would only allow a small percentage of the incident beam to be excited due to the relatively large partition function of these molecules (i.e., low population in any particular quantum state). The data primarily consist of angular distributions, velocity distributions, and intensity measurements of reflected molecules as functions of incident beam velocity, internal energy, and surface temperature. In addition to the internal energy dependence of sticking probability, results on energy accommodation and nonconservation of tangential momentum are also reported for SF_6 and Kr beams scattering from surfaces composed of their respective condensed (amorphous) ices.

EXPERIMENT

A crossed molecular beams apparatus, which is similar in design to one which has been previously described in detail,[27] was modified for this experiment by replacing one of the beam sources, and its differential pumping region, with a cryogenically cooled target surface assembly. The initial experiments involving CCl_4 utilized a liquid nitrogen cooled target mount. In subsequent studies involving SF_6 and Kr the above was replaced by a more sophisticated surface assembly which was cooled by a CTI Model-21 closed cycle helium refrigerator, producing $T_s \geq 10$ K. The underlying target substrate for both systems was fabricated from polycrystalline copper, which was prepared with a chemical polishing procedure similar to that described by Ahearn *et al.*[28] 2-mercaptobenzothiazole was used as the nitrogen containing additive in our polishing procedure.[28]

The main scattering chamber was pumped by an unbaffled 5300 ℓ/s diffusion pump using DC-705 oil, and by a liquid nitrogen cooled cold shield which was very effective in pumping condensible beam and background gases. The base pressure of the scattering chamber was 1×10^{-7} Torr during the course of these experiments. The copper "substrate" surface was therefore undoubtedly contaminated before the onset of beam condensation. However, at the surface temperatures used for data collection the sticking probability of the incident beam was always $\geq$99%, indicating that a relatively "clean" surface, consisting of an amorphous ice of the incident beam gas, was always presented to the incident molecular beam. Without UHV conditions in our main scattering chamber fairly well defined target surfaces were therefore generated via constant deposition of a large percentage of the incident beam. The reflected molecules analyzed in these experiments represented the ~1% (or less) of the incident beam flux which did not condense upon impact with the cryogenic surface.

Figure 1 is a schematic diagram which outlines the important experimental components. The effusive, heated, and velocity selected beam source constructed for this experiment permitted independent variation of T_B and ν_B, the beam temperature and beam velocity. This arrangement allowed us to examine gas–surface collisions involving polyatomic molecules having different internal energies (i.e., beam temperatures) but essentially the same translational energies (constant velocity selector frequency). The heated, effusive source consisted of a 6 mm o.d./4 mm i.d. quartz tube which was wrapped with 0.5 mm diameter tantalum wire at a turn density of 3 turns/cm. The wire heater extended from the front tip of the quartz tube to a point ca. 50 cm back from the tip in order to ensure vibrational and rotational equilibration of the quickly flowing gas with respect to the oven temperature. The orifice at the front of the tube was a slot measuring 0.75 mm×2.80 mm. A radiation shield surrounded the entire heated tube to ensure uniform heating of the oven by blackbody radiation. The true oven temperature was obtained by fitting the effusive velocity distributions produced from the source to Maxwellian distributions as a function of oven power; thermocouples implanted in the oven were calibrated against these distributions. Extreme care was taken to ensure that Maxwellian distributions were in fact generated during

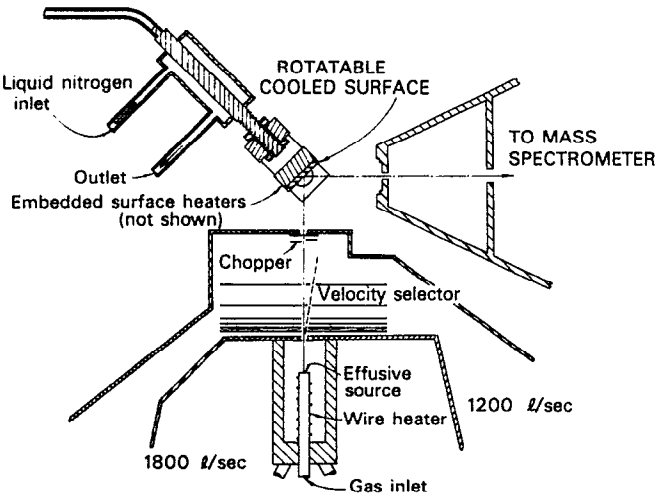

FIG. 1. Schematic diagram of the experimental scattering apparatus. In later experiments a closed-cycle helium refrigerator replaced the liquid nitrogen cooling of the target substrate.

the above oven calibration tests by running the source at very low stagnation pressures.

The velocity selector was similar to one which has been previously described.[29] It consisted of six 0.1 mm thick aluminum disks, with each disk having 160 slots of 0.081 cm width even spaced around its circumference. The average radius to the midpoint of the slots was 4.50 cm. The selector had approximately a 20% FWHM $\Delta v/v$ bandpass function and was found experimentally to have a λ conversion factor of about 201 cm, where (λ)×(wheel frequency)=most probable transmitted velocity. The overall length of the velocity selector was 2.74 cm. Absolute determination of the CCl_4 and SF_6 flux distributions transmitted by the velocity selector, as a function of oven temperature and selector frequency, was always carried out with high resolution (4 μs/chan dwell time) single-shot time-of-flight (TOF) techniques. The velocity selector could be operated at frequencies up to ~400 Hz (most probable transmitted velocity $\sim 8\times10^4$ cm/s) and the source oven temperature could be varied between room temperature and about 700 K. These T_B and ν_B ranges permitted the internal energy (E_i) to translational energy (E_t) ratio to vary over a wide range for polyatomic molecules. For the CCl_4 experiment the oven temperatures used were 298 and 560 K, and for SF_6 these temperatures were 300 and 608 K.

The CCl_4 beam was run by immersing the CCl_4 reservoir in an ice-water bath, with the resulting vapor passing through a series of needle valves before entering the beam source. Similarly, after the SF_6 was passed through a vacuum regulator its flow was throttled by a series of needle valves. The beams produced by this source were collimated by a series of apertures to a FWHM angular divergence of 2.2°.

The first generation target assembly was designed so that it could be rotated out of the beamline in order to permit the detector to look directly into the incident beam. This was believed to be necessary in order to reference the incident intensity, during the course of an experiment, as a function of oven and velocity selector settings. However, subsequent measurements of reflected angular and velocity distributions revealed that beams scattering from room temperature (dirty) copper surfaces always thermally accommodated to T_s, the surface temperature. The surface was therefore acting as a "beam normalizer" since all incident beams, regardless of their initial velocity distributions, scattered with the same final Maxwellian velocity distribution. This permitted us to design a much more precise target assembly, which did not have to rotate out of the scattering plane, when the closed-cycle refrigerator was added. For all of the experiments described in this paper the incident beam–surface angle, θ_i, was fixed at 50° from the surface normal.

The particle detector used in these studies consisted of a rotating triply differentially pumped electron bombardment ionizer/quadrupole mass spectrometer.[27] In-plane scattering events were detected, as defined by the surface normal and the incident beam, for reflected angles between 30° and 90° with respect to the surface normal. Time-of-flight velocity distributions were obtained with a post-collision chopper which was located in front of the entrance to the detector. Typical chopper to ionizer distances were 18.2 cm. For low signal experiments, conducted below the condensation point of the incident beam, cross-correlation TOF techniques[30,31] were used, employing a 255-bit, ~50% duty cycle pseudo-random chopping sequence operated at 12 μs/channel dwell time.

Angular distributions were obtained by modulating the incident beam with a 150 Hz Bulova tuning fork chopper. Repeated angular scans were taken for all angular distributions in order to achieve good signal-to-noise ratios. In the CCl_4 experiment the detected ion was CCl_3^+ while for SF_6 it was SF_5^+. These daughter ions were of higher intensity than their respective parent ions.

Finally, condensation experiments were performed under conditions having ≥99% sticking probability so that inelastic scattering events could be clearly distinguished from adsorption events followed by subsequent particle reevaporation (trapped trajectories). This was accomplished by noting that the residence times of adsorbed (trapped) molecules were several orders of magnitude larger than the gating period of the tuning fork chopper, 6.67 ms, while the interaction times of "direct" inelastically scattered molecules were much shorter, typically 10^{-12} s. In the extreme case of ≥99.9% sticking probability, virtually all of the detected molecules were directly scattered as the trapped molecules were effectively "frozen out" in the condensate. This situation was highly advantageous to our experiment as the scattering events carrying the important dynamical information were the directly scattered ones. This experiment therefore overcomes one of the main experimental difficulties associated with studying gas–surface collisions, as was briefly discussed by Zwanzig[32] in his early paper on gas–surface collisional energy transfer.

RESULTS

Angular distributions were obtained for CCl_4 and SF_6 as a function of incident velocity, internal energy, and surface temperature. The scattering behavior for these two molecules

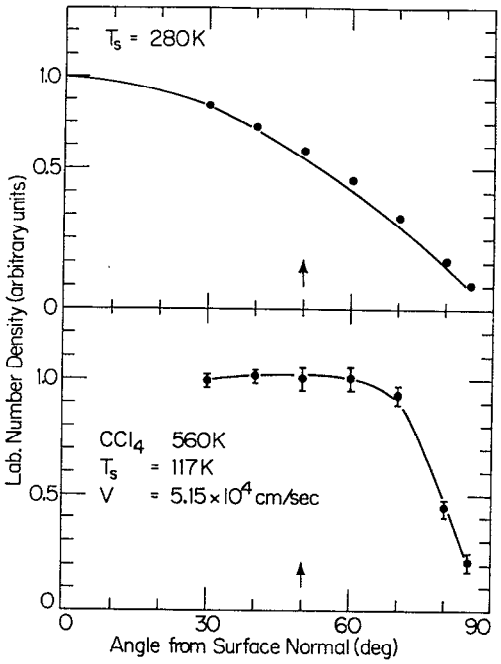

FIG. 2. Upper section: T_s=280 K CCl_4 experimental angular distribution. The solid line is a plot of the cosine (θ) function. Lower section: Angular distribution obtained at a sticking probability of ~ca. 90%. This curve exhibits characteristics belonging to both peaked and cosine scattering. The arrows indicate the specular angle in each of these figures.

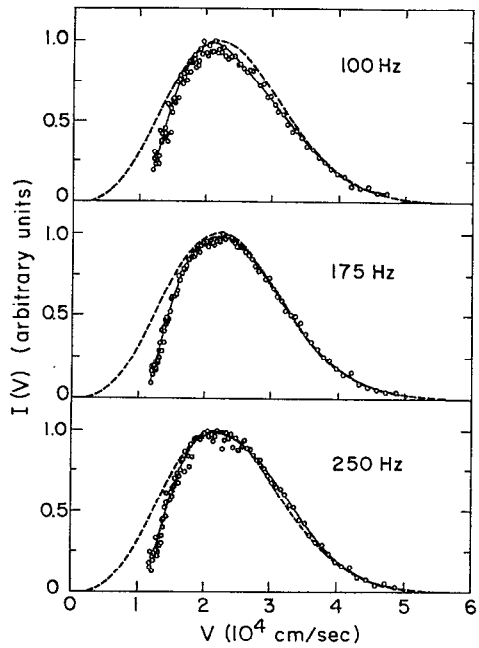

FIG. 3. Reflected velocity distributions for SF_6 scattering from a room temperature surface. The dashed lines represent Maxwellian flux distributions for 324 K. This figure confirms thermal accommodation for incident molecules. The three velocity selector frequencies correspond to mean incident translational velocities of 2.0×10^4, 3.5×10^4, and 5.0×10^4 cm/s.

was found to be quite similar, as demonstrated below. All scattered angular distributions that were measured above each molecules' respective condensation temperature were cosine in shape with respect to the surface normal. This by itself only indicates that the copper substrate was microscopically rough and that the incident beam was *possibly* thermally accommodating to T_s. The upper portion of Fig. 2 shows one of the first experimental angular distributions obtained for CCl_4 scattering from a room temperature (dirty) copper surface. In order to resolve the question of possible thermal accommodation to T_s scattered particle TOF distributions were recorded for several gases as a function of incident translational energy. The three curves shown in Fig. 3, for incident SF_6 mean velocities of approximately 2.0×10^4, 3.5×10^4, and 5.0×10^4 cm/s, conclusively demonstrate that thermal accommodation to T_s is essentially complete. The proof for this is that the three scattered particle velocity distributions, in spite of their different incident distributions, were superimposable and could be fit with a calculated 324 K Maxwellian flux distribution (dashed lines in Fig. 3). The deviations at low velocities are an artifact of the experimental TOF measurements, with the low velocity cutoff due to the finite width of the TOF chopper disk. TOF measurements for CCl_4, SF_6, and Kr revealed that thermal accommodation to the surface temperature continued with decreasing T_s until each molecule's condensation temperature was reached. This was very fortunate as it allowed us to monitor incident beam flux, as a function of velocity selector setting and oven temperature, by simply making relative reflected number density measurements as a function of these parameters at $T_s > T_c$, the condensation temperature for each molecule. (Since all reflected velocity distributions were identical, the relative number density measurements taken with our detector were equivalent to relative flux determinations.) This alleviated the need to continually remove the target surface from the beamline during the course of the experiment, as was described in the preceding section.

When the surface temperature was dropped below the CCl_4 condensation temperature [$T_c(CCl_4)\approx142$ K] to T_s=117 K a very interesting angular distribution was recorded, which is shown in the lower portion of Fig. 2. This distribution consists of some molecules which scattered with a cosine(θ) dependence, and others which scattered in a specularlike manner. As T_s=117 K corresponds to a CCl_4 sticking probability of about 90% (as determined from the counting rate at the specular angle) this view seems plausible. This indicated that still lower surface temperatures would be needed to study inelastic scattering events as the large contribution from trapped molecules (those which had been adsorbed, thermally accommodated, and subsequently reevaporated) still dominated the detected signal.

The angular distributions taken far below the CCl_4 condensation temperature exhibited a marked difference in shape from those discussed above. Figure 4 shows the angular distributions taken with T_s=90 K and T_B (oven temperature) 298 K, while Fig. 5 shows those obtained with T_B=560 K, for several different incident velocities. For CCl_4, T_s=90 K corresponds to a sticking probability of $\geq$99.5% as determined from the counting rate recorded at the specular angle. These distributions have no visible remnant of accommo-

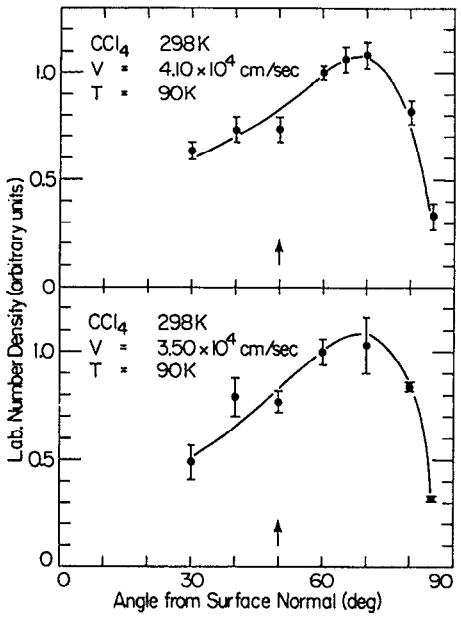

FIG. 4. Angular distributions obtained for two translational velocities with T_B=298 K. These data were taken under conditions of high sticking probability, with $S \geq 99.5\%$.

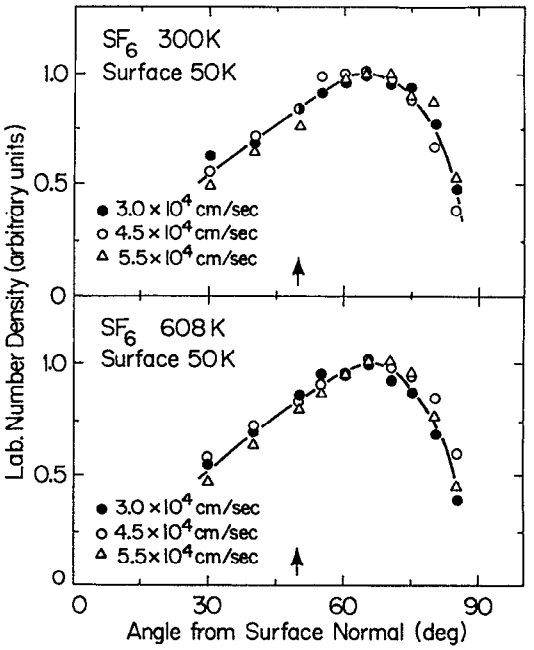

FIG. 6. Angular distributions for three different incident SF_6 velocities with T_B=300 and 608 K. These distributions were obtained in the limit of very low T_s, at a sticking probability of ≥99.5%.

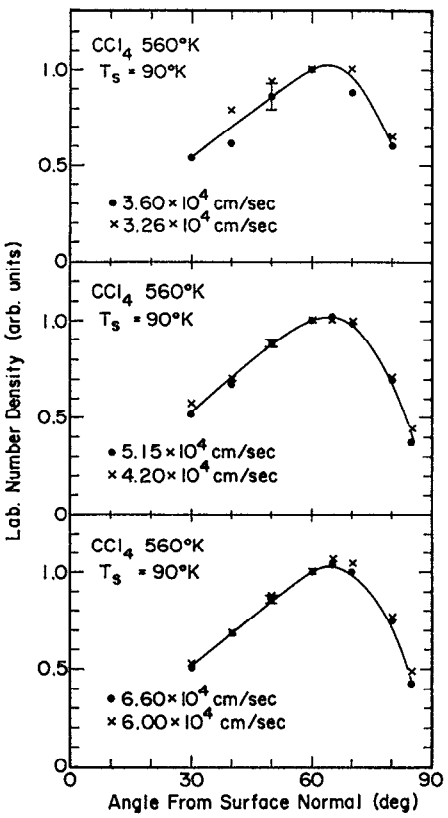

FIG. 5. Angular distributions for internally excited CCl_4 taken at a sticking probability of ≥99.5%.

dated (cosine) scattering, and peak 15° superspecularly from the specular angle of 50°. Counting rates for the distributions shown in Figs. 4 and 5 were 10 counts/s, taken with a m/e =117 background of 125 counts/s. The lack of peak scattering angle variation found in these figures, as a function of incident velocity, may imply that the CCl_4 molecules experience constant relative momentum loss collisions with the surface; however, the overall skewing of the CCl_4 angular distribution with respect to the specular angle, θ_s=50°, does indicate that momentum accommodation occurs to a greater extent in the direction perpendicular to the surface than tangential to it.

Figure 6 shows the SF_6 angular distributions that were obtained at T_s=50 K for three different incident velocities. Typical counting rates at $v_i=3\times10^4$ cm/s were 25 counts/s, with a m/e=127 background rate of 230 count/s. Signal rates were substantially higher for faster incident velocities. This surface temperature corresponds to ≥99.5% sticking probability for SF_6 at those velocities. Once again, the angular distributions do not vary very strongly with either incident velocity or beam temperature. The lack of variation with beam temperature (internal energy) may indicate a weak coupling of internal to translational energy. However, due to the relatively large mass of SF_6, only slight angular shifts would be expected.

Using cross-correlation TOF techniques the question of SF_6 energy accommodation was explored in much greater detail than during the CCl_4 experiment. The data shown in Fig. 7 represent a series of SF_6 reflected velocity distributions, taken at the specular angle, as a function of surface temperature. The dashed lines in each section of the figure represent the calculated SF_6 Maxwellian flux distributions at

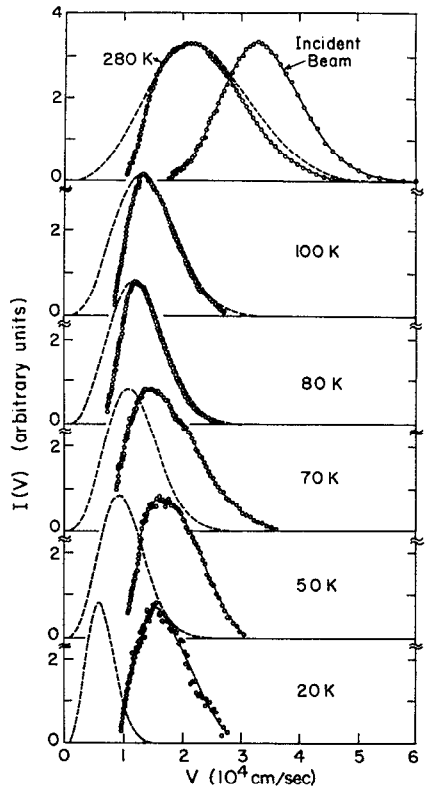

FIG. 7. Reflected SF_6 velocity distributions as a function of decreasing surface temperature. The dashed lines in each section of the figure are the calculated Maxwellian flux distributions for each T_s value. The onset of SF_6 condensation occurs at ~79 K.

each surface temperature. The experimental TOF distributions can be fit extremely well with the Maxwellian distributions for T_s=280, 100, and 80 K indicating complete SF_6 thermal accommodation to T_s. The low velocity deviations, as discussed earlier, are an artifact of the measurement. However, as the surface temperature was further lowered from 80 to 70, 50, and ultimately 20 K the experimental velocity distributions became *faster* than the Maxwellian distributions. This clearly demonstrates that we are in fact analyzing inelastic events, rather than trapped and reevaporated ones, for very low T_s values. Note also that the onset of condensation for SF_6 was found to occur at $T_c \approx 79$ K, in good agreement with the data shown in this figure.

Important information about momentum exchange and energy accommodation can be obtained from the TOF distributions shown in Fig. 7. Table I summarizes the data taken at the specular angle for SF_6 with T_B=300 K. The energy accommodation coefficients shown in this table, defined as

$$\alpha_E = \frac{E_i - E_r}{E_i - E_s}, \tag{1}$$

where E_i is the incident translational energy, E_r is the reflected beam translation energy, and E_s is the mean translational energy of a molecule at T_s, indicate that an extreme loss of energy is occurring upon impact with the surface. Analysis of the final velocity components tangent and perpendicular to the surface conclusively demonstrates that *tangential momentum is not conserved* for collisions between SF_6 and an amorphous ice surface of SF_6, ruling out an overly simplistic "hard-cube analysis"[33] of the angular distributions shown in Figs. 4, 5, and 6. The energy exchange diagram shown in Fig. 8 clarifies this point. In this figure $\tilde{\nu}_r$, θ_r, $\tilde{\nu}_i$, and θ_i are all determined experimentally. Therefore, by measuring the reflected velocity distribution at a given angle an unambiguous analysis of momentum exchange can be carried out. The α_E values listed in Table I can only be explained by assuming tangential and perpendicular momentum loss, as indicated by the solid triangle whose sides are $\tilde{\nu}_r$, $\tilde{\nu}_{tr}$, and $\tilde{\nu}_{\perp r}$ in Fig. 8. The apparent weak dependence of α_E on T_s at low surface temperatures (i.e., in the limit of preferentially removing all thermally accommodated SF_6) indicates that impulsive collisions are dominating the scattering.

TABLE I. SF_6 energy accommodation.

T_s (K)	α_E	$\langle E_r\rangle/\langle E_i\rangle$	$\langle E_r\rangle/\langle E_s\rangle$
70	0.82	0.29	2.21
50	0.77	0.30	3.18
20	0.77	0.25	6.79

Similar data were obtained for Kr scattering from krypton ice as a function of T_s. This is shown in Fig. 9 and briefly summarized in Table II. Once again the reflected velocity distributions have much higher average velocities than thermally accommodated ones for surface temperatures lower than the beam condensation temperature [T_c(Kr)<40 K]. Analysis of the reflected velocity distributions also indicate that tangential momentum is not conserved. The slight deviation of the 40 K experimental TOF distribution from the theoretical curve on its high velocity side may be real, and can possibly be explained by microscopic reversibility argu-

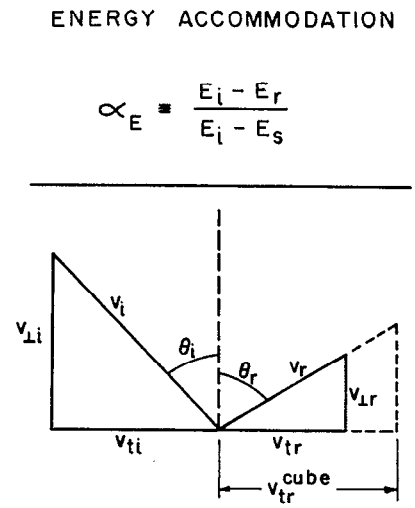

FIG. 8. Schematic velocity diagram for gas–surface scattering events. $\tilde{\nu}_{tr}^{cube}$ represents the tangential velocity vector within the hard-cube approximation.

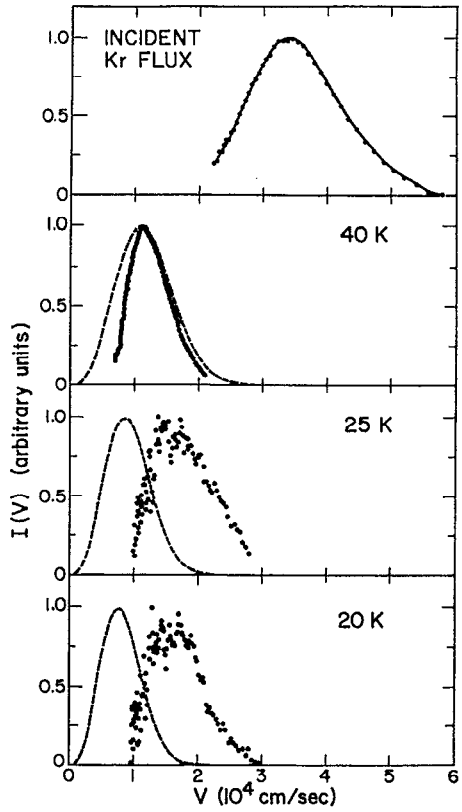

FIG. 9. Reflected krypton velocity distributions as a function of surface temperature, taken at the specular angle. The dashed lines in each section of the figure are the calculated Maxwellian flux distributions for each T_s value.

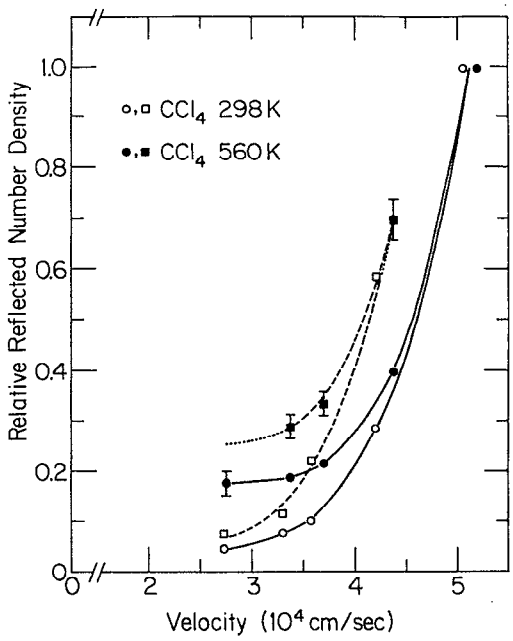

FIG. 10. CCl_4 reflection probability as a function of incident velocity for T_B=298 and 560 K. The dashed lines and related square symbols are the deconvoluted reflection probability curves for which the finite bandpass function of the velocity selector has been taken into account

ments. One might expect evaporating particles to be slightly deficient in high velocity events since the condensation probability for fast incident particles is less than that for slowly incident ones.

Finally, and most importantly, we have conducted an extensive investigation of how translational and internal energy influence the sticking probability of CCl_4 and SF_6 for collisions involving these molecules and their respective condensed phases. In Fig. 10 the relative reflection probability for CCl_4, as a function of incident velocity, is shown for two different oven temperatures (internal energies), T_B=298 K and T_B=560 K. These curves were generated by measuring the relative reflected flux, as a function of velocity selector setting, for T_s=90 K. More specifically, the experimental data points were obtained by normalizing the reflected number density detected at a given angle, as a function of oven temperature and velocity selector setting, to the incident beam flux for the same values of ν_i and T_B.

TABLE II. Krypton energy accommodation.

T_s (K)	α_E	$\langle E_r\rangle/\langle E_i\rangle$	$\langle E_r\rangle/\langle E_s\rangle$
40	0.99	0.14	1.09
25	0.77	0.29	3.75
20	0.79	0.26	4.11

Two clear trends can be seen from the data shown here. First, reflection probability has a very strong dependence on incident translational energy, with the probability of reflection increasing dramatically with increasing incident velocity. Second, *the relative reflection probability curves for two different internal energies differ at low incident velocities, and asymptotically merge with each other in the limit of high incident velocity.* This is the first indication that the internal energy (i.e., the energy stored in rotation and vibration) of a polyatomic molecule can influence its sticking probability, S, where RP (reflection probability)$\equiv 1-S$.

The above results, obtained as a function of velocity selector frequency, need to be deconvoluted with respect to the bandpass function of the selector since the transmitted velocity distributions were fairly wide, having a FWHM $\Delta\nu/\nu$ of about 20%. This was accomplished using an iterative, ratio method deconvolution procedure. Following the basic form of Siska's iterative deconvolution procedure[34] we have

$$f_0(\nu)=h(\nu), \tag{2}$$

$$f_{n+1}(\nu)=f_n(\nu)[h(\nu)/g^*f_n], \tag{3}$$

where, in our case, $h(\nu)$ is the experimental (folded) reflection probability for a given velocity selector setting, $g(\nu,\nu')$ is the experimentally determined velocity selector transmission function, and $f_n(\nu)$ is the nth deconvoluted (unfolded) approximation to $h(\nu)$. The actual convolution integral, g^*f, was defined as

$$g^* f_{n+1} = \int_{\nu_i}^{\nu_f} d\nu'\ g(\nu,\nu') f_n(\nu') \approx \sum_{i=1}^{n} g(\nu,\nu') f_n(\nu') \tag{4}$$

where ν_i and ν_f are the initial and final velocities transmitted by the selector at a given frequency. The actual $g(\nu,\nu')$ distributions were obtained with high resolution single-shot TOF operating at 4 μs/channel dwell time. The convolution integral was calculated with trapezoidal rule numerical integration. Each successive $h(\nu)$ was generated by least squares fitting a fourth-order polynomial to $f_n(\nu)$, where $f_n(\nu) = \mathrm{RP}_n(\nu)$. After a few iterations, typically 3–5 cycles, the deconvolution procedure converged, and was tested by refolding $f_{n,\mathrm{final}}(\nu)$ with $g(\nu,\nu')$

$$g^* f_{n,\mathrm{final}} = \int_{\nu_i}^{\nu_f} d\nu'\ g(\nu,\nu') f(\nu') \approx h(\nu). \tag{5}$$

For most velocity ranges it was found that the refolded distribution, $g^* f_{n,\mathrm{final}}$, virtually reproduced the experimental data, indicating a successful deconvolution. However, for relatively fast velocities ($\nu \geq 4.5\times10^4$ cm/s) the deconvolution routine experienced difficulties since a very strong function of velocity, RP(ν), was being folded with a fairly broad bandpass function. The dashed lines shown in Fig. 10 represent the results of this RP(ν) deconvolution for CCl_4.

The internal energy dependence of condensation probability can be expressed in a quantitative manner by plotting the ratio of the reflection probability curves, for different oven temperatures, as a function of incident velocity. We have explicitly calculated the reflection enhancement factor, EF, which is actually the ratio of relative reflected fluxes for molecules having the same translational velocity, ν_i, and different internal energies

$$\mathrm{EF}(T_s = 90\mathrm{K}, \nu_i) = \frac{(\text{Fraction of flux reflected}; T_B = 560\mathrm{K})}{(\text{Fraction of flux reflected}; T_B = 298\mathrm{K})} = \frac{\left(\dfrac{n_r^{90} v_r^{90}}{\text{Incident flux}(T_B;\nu_i)}\right)\Bigg|_{T_B=560\mathrm{K}}}{\left(\dfrac{n_r^{90} v_r^{90}}{\text{Incident flux}(T_B;\nu_i)}\right)\Bigg|_{T_B=298\mathrm{K}}}, \tag{6}$$

where n_r^{90} and v_r^{90} are the reflected number densities and velocities at $T_s = 90$ K for each beam temperature. Figure 11 shows the EF values determined for CCl_4, which were obtained from Fig. 10 using Eq. (6). The solid line in Fig. 11 corresponds to the reflection enhancement factor that was calculated with the experimental RP(ν) curves, while the dashed line corresponds to the deconvoluted result. *The EF curves shown in this figure conclusively demonstrate that internal excitation of a molecule's rotational and vibrational degrees of freedom leads to an increase in its reflection probability (decrease in sticking probability) in the limit of low incident velocity.* EF$\approx$4 implies that internally excited CCl_4 molecules with $\langle\nu_i\rangle \approx 2.7\times10^4$ cm/s are four times more likely to scatter from the CCl_4 ice surface than vibrationally and rotationally "cool" ones. Furthermore, the EF curves shown in this figure indicate that in the limit of high incident velocities EF goes asymptotically to unity, indicating that

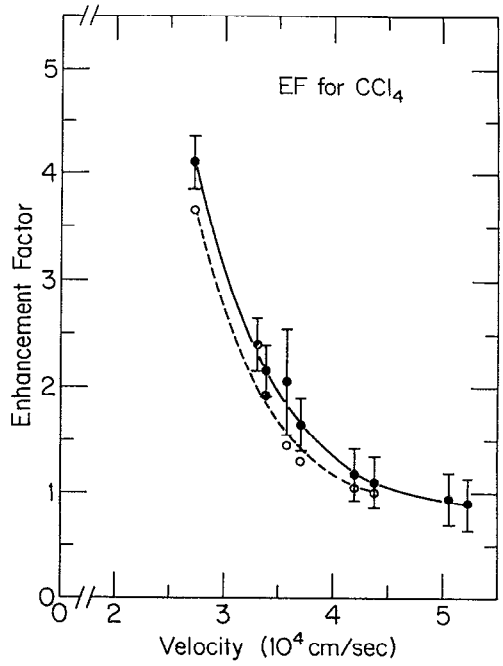

FIG. 11. Internal energy reflection enhancement factor curve for CCl_4 as a function of incident velocity. EF=4 implies that internally hot (560 K) CCl_4 molecules have a four times higher probability of being reflected from a cold (90 K) surface than do room temperature molecules. The dashed line and related open circles mark the deconvoluted EF curve for which the finite bandpass function of the velocity selector has been taken into account.

internal excitation has little influence upon condensation probability for high velocity particles. This will be discussed in detail in the next section of this paper. Note that the actual v_r^{90} values which appear in Eq. (6) were not experimentally determined here (i.e., for CCl_4), and that the EF values shown in Fig. 11 were calculated assuming equal reflected velocities for scattered molecules which had the same incident velocities but differing internal energies. In reality, the scattered molecules which were initially internally excited may scatter with slightly larger reflected velocities. The EF values of Fig. 11 may therefore be viewed as lower bound estimates for enhanced scattering due to internal excitation.

Figures 12 and 13 show, respectively, the reflection probability curves and reflection enhancement factors for SF_6 with oven temperatures of 300 and 608 K, and $T_s = 50$ K, as a function of incident velocity. The solid lines once again correspond to the experimental distributions while the dashed lines are the deconvoluted results. The qualitative shapes of these curves are quite similar to those for CCl_4, indicating that internal excitation can inhibit condensation in the limit of low incident translational energy. The velocity range explored in these experiments could not be extended to include velocities lower than about 2.5×10^4 cm/s or higher than 5.5×10^4 cm/s due to the extremely low signal level of the $T_B \sim 300$ K data in these velocity regimes. The RP(ν) and EF(ν) curves shown in Figs. 10–13 are the main results of this series of beam–surface scattering experiments.

Extreme care was taken to guarantee that these reflection probability distributions were not an artifact of some system-

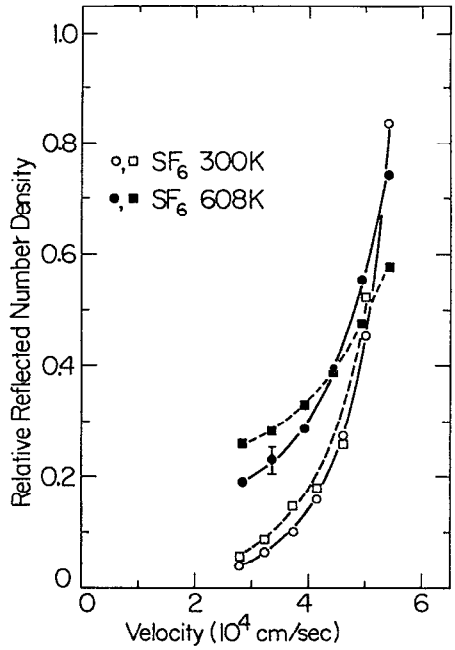

FIG. 12. SF_6 reflection probability as a function of incident velocity for T_B=300 and 608 K. The dashed lines and related square symbols are the deconvoluted reflection probability curves for which the finite bandpass function of the velocity selector has been taken into account.

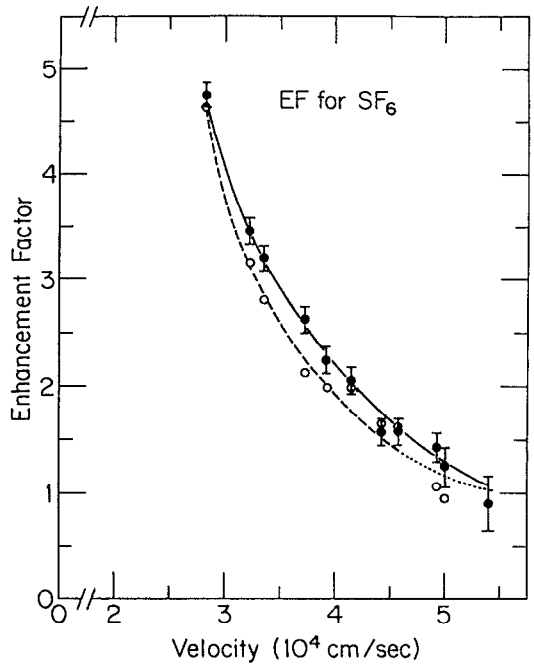

FIG. 13. Internal energy reflection enhancement factor curve for SF_6 as a function of incident velocity. The dashed line and related open circles mark the deconvoluted EF curve for which the finite bandpass function of the velocity selector has been taken into account. The dotted line is an extrapolation of the deconvoluted EF curve to v_i=5.5×10^4 cm/s.

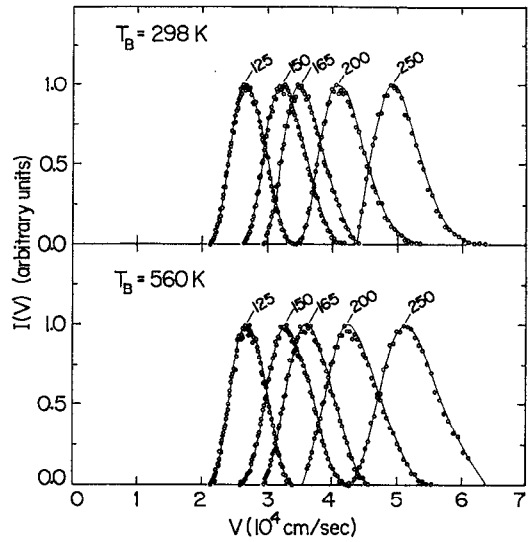

FIG. 14. Experimentally determined CCl_4 incident flux distributions, as a function of velocity selector frequency, for T_B=298 and 560 K.

atic error. The reflection probability was monitored in a series of tests as a function of beam intensity, and was found to linearly track the beam intensity. This indicated that impurities on the surface (from background gas in the scattering chamber) were not significantly affecting the results. More importantly, the actual transmitted velocity distributions for the hot and room temperature source settings were not always superimposable for the same velocity selector frequency. This occurred since the bandpass function of the selector was folded with the shape of the flux distribution effusing from the quartz slot. At high velocities the long tail of the high temperature flux distributions skewed the transmitted velocity distributions to higher velocities. Figures 14 and 15 show the actual incident CCl_4 and SF_6 velocity distributions, as a function of velocity selector frequency, for

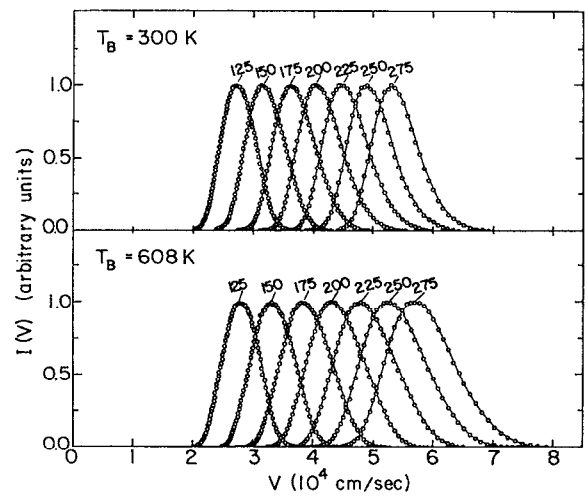

FIG. 15. Experimentally determined SF_6 incident flux distributions, as a function of velocity selector frequency, for T_B=300 and 608 K.

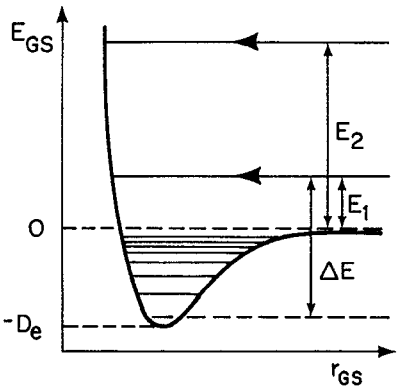

FIG. 16. Schematic energy diagram of a gas–surface interaction potential.

both room temperature and elevated source temperatures. These distributions were obtained by taking TOF measurements with the detector looking directly into the incident beam transmitted at a given velocity selector setting. The low frequency (slow) distributions for hot and room temperature beams are superimposable for both CCl_4 and SF_6, while at higher frequencies the hot distributions are noticeably skewed to higher velocities. The virtual overlap of the low frequency distributions for different source temperatures is quite fortunate as the low velocity data points in Figs. 10–13 are the most crucial ones for supporting the presence of internal energy effects. Nevertheless, the experimental EF curves shown in Figs. 11 and 13 have been corrected for these shifts, and the successful deconvolution of the data with respect to the actual incident distributions exactly corrected for the problem.

DISCUSSION

The results shown in the preceding section clearly indicate that the internal energy of a polyatomic molecule becomes increasingly more important in determining its sticking probability as its translational energy is decreased. This can be understood in terms of the energy loss which must occur in the direction perpendicular to the surface for condensation to occur. A simple energy level schematic for gas–surface scattering is shown in Fig. 16. The potential energy well in this figure represents the gas–surface interaction potential, E_1 and E_2 represent low and high energy incident trajectories referenced to the dissociation limit of the gas–surface potential, and ΔE, as drawn, indicates the total energy loss which ultimately occurs for the E_1 trajectory if it becomes trapped and subsequently accommodated to T_s, for low T_s values. In this simplified picture of the condensation process the extent of *initial* energy loss in the direction normal to the surface determines whether a particle becomes trapped, and subsequently accommodated to T_s, or whether it will inelastically scatter from the surface. For trapping to occur the low and high energy trajectories must lose at least E_1 and E_2, respectively, upon initial impact with the repulsive wall of the gas–surface interaction potential. (*This view is of course oversimplified as multiple collisions, such as those in a tumbling encounter, may also contribute to energy transfer and, ultimately, trapping.*) Energy losses less than these critical amounts will lead to "direct inelastic" scattering events which have a strong memory of their initial state. As the translational energy of an incident molecule is increased we therefore see that increasingly more energy must be lost in the initial collision for condensation to occur. The steadily decreasing probability that this threshold energy loss will occur gives rise to the RP(v) curves shown in Figs. 10 and 12 for CCl_4 and SF_6. In the limit of *high* incident translational energy we would therefore expect that coupling of internal energy (rotation, vibration) to translation upon impact with the repulsive wall of the gas–surface potential (i.e., $V,R \rightarrow T$ collisional energy transfer) would have very little influence on the condensation probability for the molecule. Conversely, this overview of the condensation process seems to indicate that any collisional V, $R \rightarrow T$ energy exchange for *low kinetic energy* incident molecules would lead to a significant decrease in sticking probability, as is experimentally found, as shown in Figs. 11 and 13.

Since gaseous condensation is essentially a problem of translation accommodation, it is interesting to compare the relative effectiveness of internal and translational energy for inhibiting sticking. Using the vibrational quantum partition function for an ideal polyatomic molecule, the mean vibrational energy difference between CCl_4 at 298 and 560 K is found to be ca. 3.7 kcal/mol, while the rotational energy change between these two temperatures is well approximated by 3/2 $k\Delta T$, or ca. 0.8 kcal/mol. In going from 2.7×10^4 to 5.0×10^4 cm/s the CCl_4 translational energy increases from about 1.3 to 4.5 kcal/mol. Over this velocity range the deconvoluted $T_B=300$ K, RP(v) curve for CCl_4 increased by a factor of about 15, while the largest EF found was only about 4. Therefore translational energy appears to be more "efficient" per unit of energy than internal energy in inhibiting condensation. This comparison is not totally fair as all of the internal modes certainly do not collisionally couple to translation upon impact. However, the trend outlined above is representative of the behavior exhibited by relatively large polyatomic molecules. Similar calculations for SF_6 lead to the same qualitative result as above. The increase in vibrational energy for SF_6 in going from $T_B=300$ to 608 K is found to be about 8.3 kcal/mol, while the gain in rotational energy is 0.9 kcal/mol. Similarly its translational energy increases from 1.3 to 4.4 kcal/mol upon increasing its mean incident velocity from 2.7×10^4 to 5.0×10^4 cm/s. The SF_6 RP(v) curve for $T_B=300$ K increased by a factor of ~10 over this translational energy range, while EF for the most favorable case was only about 4.6.

Finally, our findings emphasize that the internal energy reflection enhancement factor should be treated theoretically with a dynamic, collisional energy transfer description akin to gas-phase and gas–surface inelastic scattering models. Adsorption–re-evaporation models[1,3] are inadequate for describing the results found in this experiment.

CONCLUSION

Molecular beam surface scattering experiments have been carried out which have shown that the internal energy

of a molecule can significantly influence its sticking probability upon collision with an amorphous ice of its own condensed phase. This internal energy effect is greatest for molecules having relatively low incident translational energies, and essentially vanishes at higher velocities. For CCl_4 and SF_6 the largest reflection enhancement factors, EF, found were, respectively, 3.7 and 4.6 (with EF defined as the ratio of reflected fluxes for molecules having different internal energy content but traveling with the same incident kinetic energy). Reflected particle velocity analysis carried out with cross-correlation time-of-flight techniques has revealed that a very large degree of translational energy accommodation is occurring for inelastically scattered SF_6 molecules, with thermal accommodation coefficients, α_E, as large as 0.77 being achieved. The weak surface temperature dependence of α_E for Kr and SF_6 in the limit of low surface temperature implies that impulsive collisions are dominating the observed scattering events. Tangential momentum is not conserved in these collisions. Finally, these studies were conducted in the limit of very high sticking probability ($\geq$99%) so that the trapped (accommodated) molecules would be essentially frozen out upon impact with the surface, leaving only the "direct inelastic" scattering events contributing to the detected signal. This condition is highly advantageous as the directly scattered molecules contain the important energy exchange and collision dynamics information sought after in this experiment. Our findings suggest that heterogeneous laser isotope separation schemes based on precollision molecular excitation may warrant further investigation.

ACKNOWLEDGMENTS

S.J.S. thanks JILA at the University of Colorado, Boulder for a Visiting Fellowship and hospitality which assisted the preparation of this manuscript. This work was supported by the Director, Office of Energy Research, Office of Basic Energy Sciences, Chemical Sciences Division of the U.S. Department of Energy under Contract No. DE-AC03-76SF00098.

[1] K. S. Gochelashvili, N. V. Karlov, A. N. Orlov, R. P. Petrov, Yu. N. Petrov, and A. M. Prokhorov, Zh. Eksp. Teor. Fiz. Pis. Red. **21**, 640 (1975) [JETP Lett. **21**, 302 (1975)].
[2] N. V. Karlov and K. V. Shaitan, Zh. Eksp. Teor. Fiz. **71**, 464 (1976) [Sov. Phys. JETP **44**, 244 (1976)].
[3] J. D. Doll, J. Chem. Phys. **66**, 5709 (1977).
[4] N. F. Basov, E. M. Belenov, V. A. Isakov, Yu. S. Leonov, E. P. Markin, A. N. Oraevskii, V. I. Romanenko, and N. B. Ferapontov, Zh. Eksp. Teor. Fiz. Pis. Red. **22**, 221 (1975) [JETP Lett. **22**, 102 (1975)].
[5] K. S. Gochelashvili, N. V. Karlov, A. I. Ovchenkov, A. N. Orlov, R. P. Petrov, Yu. N. Petrov, and A. M. Prokhorov, Zh. Eksp. Teor. Fiz. **70**, 531 (1976) [Sov. Phys. JETP **43**, 274 (1976)].
[6] G. K. Anderson and J. T. Lee, Opt. Lett. **3**, 10 (1978).
[7] A. Gelb and M. J. Cardillo, Surf. Sci. **64**, 197 (1977).
[8] M. Balooch, M. J. Cardillo, D. R. Miller, and R. E. Stickney, Surf. Sci. **46**, 358 (1974).
[9] M. J. Cardillo, M. Balooch, and R. E Stickney, Surf. Sci. **50**, 263 (1975).
[10] J. Harris, Surf. Sci. **221**, 335 (1989).
[11] M. R. Hand and S. Holloway, J. Chem. Phys. **91**, 7209 (1989).
[12] W. Brenig and H. Kasai, Surf. Sci. **213**, 170 (1989).
[13] W. Brenig, S. Küchenhoff, and H. Kasai, Appl. Phys. A **51**, 115 (1990).
[14] B. E. Hayden and C. L. A. Lamont, Phys. Rev. Lett. **63**, 1823 (1991).
[15] B. E. Hayden and C. L. A. Lamont, Surf. Sci. **243**, 31 (1991).
[16] H. F. Berger, M. Leisch, A. Winkler, and K. D. Rendulic, Chem. Phys. Lett. **175**, 425 (1990).
[17] H. F. Berger and K. D. Rendulic, Surf. Sci. **253**, 325 (1991).
[18] C. T. Rettner, D. J. Auerbach, and H. A. Michelsen, Phys. Rev. Lett **68**, 1164 (1992).
[19] C. N. Stewart and G. Ehrlich, J. Chem. Phys. **62**, 4672 (1975).
[20] J. T. Yates, Jr., J. J. Zinck, S. Sheard, and W. H. Weinberg, J. Chem. Phys. **70**, 2266 (1979).
[21] S. G. Brass, D. A. Reed, and G. Ehrlich, J. Chem. Phys. **70**, 5244 (1979).
[22] C. T. Rettner, H. E. Pfnür, and D. J. Auerbach, J. Chem. Phys. **84**, 4163 (1986).
[23] S. T. Ceyer, Ann. Rev. Phys. Chem. **39**, 479 (1988).
[24] H. Vach, J. Hager and H. Walther, J. Chem. Phys. **90**, 6701 (1989).
[25] B. D. Kay and T. D. Raymond, J. Chem. Phys. **85**, 4140 (1986).
[26] S. J. Sibener and Y. T. Lee, *Proceedings of the XIth Intern. Symp. on Rarefield Gas Dynamics*, edited by R. Campargue (Commissariat A L'Energie Atomique, Paris, 1979), pp. 1417–1426.
[27] Y. T. Lee, J. D. McDonald, P. R. LeBreton, and D. R. Herschbach, Rev. Sci. Instrum. **40**, 1402 (1969).
[28] J. S. Ahearn, Jr., J. P. Monaghan, Jr., and J. W. Mitchell, Rev. Sci. Instrum. **41**, 1853 (1970).
[29] T. P. Schafer, Ph.D. dissertation, the University of Chicago, Chicago, Illinois, 1972.
[30] K. Sköld, Nucl. Instrum. Meth. **63**, 114 (1968).
[31] V. L. Hirschy and J. P. Aldridge, Rev. Sci. Instrum. **42**, 381 (1971).
[32] R. W. Zwanzig, J. Chem. Phys. **32**, 1173 (1960).
[33] R. M. Logan and R. E. Stickney, J. Chem. Phys. **44**, 195 (1966).
[34] P. E. Siska, J. Chem. Phys. **59**, 6052 (1973).